arXiv:cond-mat/0310680v1 [cond-mat.stat-mech] 29 Oct 2003

Steady-State Properties of a Totally Asymmetric Exclusion Process with Periodic Structure

Greg Lakatos,[1,*] Tom Chou,[2,†] and Anatoly Kolomeisky[3,‡]

[1]*Department of Physics, University of British Columbia, Vancouver, BC, Canada, V6T-1Z1*
[2]*Department of Biomathematics, UCLA, Los Angeles, CA 90095-1766*
[3]*Department of Chemistry, Rice University, Houston, TX 77251-1892*

(Dated: February 2, 2008)

We formulate and analyze the steady-state behavior of totally asymmetric simple exclusion processes (TASEPs) that contain periodically varying movement rates. In our models, particles at a majority sites hop to the right with rate p_1 while particles occupying a periodically arranged set of sites move to the right at rate p_2. A number of approximate mean field approaches are used to study the steady-state currents and bulk densities of this model. While exact solutions are not found, the mean field approaches provide results that show good agreement with data derived from extensive Monte-Carlo simulations.

PACS numbers: 05.70.Ln,05.60.Cd,05.10.Gg,02.50.Ey,02.70.Uu

I. INTRODUCTION

As a canonical model of one-dimensional transport, the Totally Asymmetric Simple Exclusion Process (TASEP) is a topic of current interest. One of the few solvable non-equilibrium models, the TASEP and its solutions have been extensively investigated [1, 2, 3, 4, 24] as a model for numerous one-dimensional transport processes including ribosome motion [5, 6, 7], pore transport [8], and traffic flow [9, 10]. The traditional TASEP model consists of a finite lattice with open boundaries. Particles are inserted into an empty site at the leftmost end of the lattice at a rate α, and once in the lattice the particles move to the right at a rate p. Each motion of a particle within the lattice moves that particle exactly one lattice site to the right, and particles can move only if the site immediately to the right is not occupied by another particle. Upon reaching the rightmost lattice site, particles are removed from the lattice at a rate β. Exact solutions for the steady-state particle currents (J), and densities (σ), are available through mean field approaches [1, 5], matrix product methods [2], and recurrence relations [4]. The latter two approaches solve the model completely, providing exact expressions for density correlation functions of arbitrary order. The TASEP solution itself yields a phase diagram with three phases. At large values of the injection (α) and extraction (β) rates the system is dominated by the rate of particle hopping and is in a maximal current phase. At small values of α and β, the system is found in a low-density entry limited phase, and a high-density exit-limited phase respectively. Within each of these two boundary-limited phases lie a pair of sub-phases each with a distinct density profile. The fundamental form of this phase diagram has proven to be very robust and extending the TASEP to include particles that occlude more than one lattice site [6], or backwards particle motions [3], has not altered the phase diagram significantly. Nonetheless, these extensions have facilitated the use of the TASEP in modeling a wide variety of physical processes. In many phenomena of interest however, the assumption of a single internal hopping rate p implicit in the normal TASEP does not adequately capture the full character of the transport behavior. One system that has been the subject of intense interest is the kinesin motor protein and related molecules [11]. Kinesin, and kinesin-like molecules, form an integral part of the cellular transport system, shuttling protein-filled lipid vesicles to various parts of the cell. Traveling along tubulin polymers, the motion of the kinesin molecule is driven by a complex conformational change producing steps approximately 8nm in length [12]. The exact stepping mechanism of the kinesin family of motor proteins is currently the subject of speculation, however one of the leading candidate models is the so-called "inchworm" model [13]. The inchworm model proposes that a single 8nm step is composed of two sub-steps; in the first sub-step one kinesin head group moves from its current position to the next available binding site on the tubulin filament. This sub-step is immediately followed by a dragging motion where the lagging head group is pulled up to essentially the same position as the lead group.

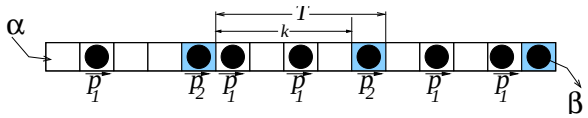

FIG. 1: The two-rate totally asymmetric exclusion model. At every T lattice sites, the particle movement rate is p_2. At all intervening sites, the movement rate is p_1. All other aspects of the model are identical to those of the standard TASEP.

While TASEP models have been successfully applied to model molecular motor dynamics in the past [14], apply-

*Electronic address: glakatos@physics.ubc.ca
†Electronic address: tomchou@ucla.edu
‡Electronic address: tolya@rice.edu

ing the TASEP to the two-part motion of the inchworm model requires that the TASEP be extended. As the two sub-steps in the inchworm model are not expected to occur at the same rate we can expand the applicability of the TASEP to these types of systems by introducing two internal hopping rates p_1, and p_2 (cf. Fig. 1) into the TASEP model. We assign these hopping rates to the lattice sites in an alternating fashion where odd indexed lattice sites move particles to the right with rate p_1, while even indexed sites move particles with rate p_2. Using this arrangement a single (p_1, p_2) unit would comprise, for example, a 8nm kinesin step with the p_1 step representing the movement of the lead head group, and the p_2 step the movement of the trailing group. Generalizing this two-rate TASEP model, we also consider the case where the p_2 sites are separated by an arbitrary number (k) of p_1 sites. Applying mean field methods we develop accurate approximations to the steady-state current and density of the dual-rate TASEP in the maximal current phase, entry limited, and exit limited regimes. We also conjecture that, as was true with many previous extensions to the standard TASEP, the dual-rate extension does not fundamentally alter the form the TASEP phase diagram. The accuracy of our mean field methods are verified through extensive Monte Carlo simulations.

II. MEAN FIELD THEORIES

A. Simple Mean Field Methods

We begin by considering the dual-rate TASEP in the limit of large α and β. As is the case in the standard TASEP, the dynamics of the system will be determined entirely by the internal movement rates p_1 and p_2. Ensuring continuity of the current in a lattice with k p_1 sites between each p_2 site we find

$$J = p_2\sigma_{k+1}(1-\sigma_1) = p_1\sigma_k(1-\sigma_{k+1}) = \dots \quad (1)$$

In writing Eqn (1) we have assumed that the densities (σ_i) in the lattice have the same period $(T \equiv (k+1))$ as the movement rates in the lattice [25]. Moreover, as the two-rate TASEP preserves the particle-hole symmetry found in the standard TASEP, we expect for a lattice of size N that $\sigma_i = (1-\sigma_{N-i+1})$ [24]. Coupling this condition to the assumption of periodicity in the densities, we find that within a single period, $\sigma_i = (1-\sigma_{k-i+2})$. Thus we can immediately eliminate half the variables in (1). While straight-forward to solve, (1) yields increasingly unwieldy expressions for the current and the densities as k increases. As a result we only show the result for the $k = 1$ case:

$$\begin{aligned} J &= \frac{p_1 p_2}{\left(\sqrt{p_1}+\sqrt{p_2}\right)^2} \\ \sigma_1 &= \frac{\sqrt{p_2}}{\sqrt{p_1}+\sqrt{p_2}} \\ \sigma_2 &= \frac{\sqrt{p_1}}{\sqrt{p_1}+\sqrt{p_2}} \end{aligned} \quad (2)$$

These relations show the expected invariance under the interchange of p_1 and p_2. To find the boundary limited currents in the simple mean field approximation we assume that at least one of α or β is less than the smaller of p_1 and p_2. For the sake of simplicity, we also assume the lattice is composed of a whole number of periods, so that the last lattice site is a p_2 site. Focusing initially on the entry-limited case and applying the current continuity conditions we find, for arbitrary k

$$J = \alpha(1-\sigma_1) = p_1\sigma_1(1-\sigma_2) = \dots = p_2\sigma_{k+1}(1-\sigma_1) \quad (3)$$

Yielding the following densities and currents for the $k = 1$ case:

$$\begin{aligned} J_\alpha &= \alpha(1-\sigma_1) = p_1\sigma_1(1-\sigma_2) = p_2\sigma_2(1-\sigma_1) \\ \Rightarrow \quad J_\alpha &= \frac{p_1(p_2-\alpha)\alpha}{p_2(p_1+\alpha)-\alpha p_1} = \alpha(1-\sigma_1) \\ \sigma_1 &= \frac{\alpha p_2}{p_2(p_1+\alpha)-\alpha p_1} \\ \sigma_2 &= \alpha/p_2 \end{aligned} \quad (4)$$

Similarly in the exit limited case we have

$$\begin{aligned} J &= p_1\sigma_{N-T}(1-\sigma_{N-T+1}) = p_1\sigma_{N-T+1}(1-\sigma_{N-T+2}) \\ &= \dots = p_1\sigma_{N-1}(1-\sigma_N) = \beta\sigma_N \end{aligned} \quad (5)$$

$$\begin{aligned} J_\beta &= \beta(\sigma_2) = p_1\sigma_1(1-\sigma_2) = p_2\sigma_2(1-\sigma_1) \\ \Rightarrow \quad J_\beta &= \frac{p_1(p_2-\beta)\beta}{p_2(p_1+\beta)-\beta p_1} \\ \sigma_1 &= 1-\frac{\beta}{p_2} \\ \sigma_2 &= \frac{p_1(p_2-\beta)}{p_2(p_1+\beta)-p_1\beta} \end{aligned} \quad (6)$$

To determine the transitions between the maximal current and entry limited regions we equate the maximal current solutions generated by (1) to the expressions for J_α and J_β in (3) and (5) to find the boundaries between the entry/exit limited and maximal current phases (α^*, β^*). For the $k = 1$ case this yields

$$\alpha^* = \beta^* = \frac{\sqrt{p_1}p_2}{\sqrt{p_1}+\sqrt{p_2}} \quad (7)$$

Finally equating the the current expressions in equations (3) and (5) we find that the transition between the entry and exit limited regions occurs when $\alpha = \beta$.

B. Refined Mean Field Methods

While appealingly transparent, we will see in the next section that the results of the simple mean field approach do not provide a particularly good match to the results of Monte Carlo simulations.

We attribute the poor performance of the simple mean field method to the method's failure to capture the correlations between the occupation probabilities of different lattice sites. To address this deficiency we apply two alternative mean field approaches. The first refined mean field, which we call the *finite-segment* method (FSMFT), involves exactly solving the master equation for a finite segment of the dual-rate TASEP lattice in a self-consistent manner (see Appendix A). While primarily numerical in nature, this method can produce estimates for the current and density comparable to the results from MC simulations. The quality of the estimates produced by the FSMFT approach is a function of the length of the finite-segment, with longer segments producing superior results.

The second enhanced mean field method is an extension to the two hopping rate TASEP of the well-known cluster mean field approach described in [9] and [15]. This method tries to capture the occupancy correlation between adjacent sites by solving the exact master equation for the multi-site probabilities $P(\tau_i, \tau_{i+1}, \tau_{i+2}, \ldots)$. As before τ_i refers to the instantaneous occupancy of site i (see Appendix B). As is typically the case, the cluster mean-field method becomes increasingly unwieldy as the size of the cluster increases. The results for the $k = 1$ case are

$$\sigma_1 = \frac{p_1 + 2p_2}{3(p_1 + p_2)},\ \sigma_2 = \frac{2p_1 + p_2}{3(p_1 + p_2)},\ J = \frac{p_1 p_2}{2(p_1 + p_2)} \tag{8}$$

As expected, the solutions are invariant under the exchange $(\sigma_1, p_1) \leftrightarrow (\sigma_2, p_2)$, and regenerate the standard TASEP results in the limit $p_1 = p_2$. We note that in the maximal current solution, $\sigma_1 + \sigma_2 = 1$ as a consequence of the particle-hole symmetry in the model.

Finally, note that we can use these results to predict the location of the phase boundary between the maximal current and entry limited phases. Using the results for the densities in the maximal current phase and applying current continuity at the entrance of the lattice we find

$$\begin{aligned} \alpha^*(1 - \frac{p_1 + 2p_2}{3(p_1 + p_2)}) &= \frac{p_1 p_2}{2(p_1 + p_2)} \\ \Rightarrow \quad \alpha^* &= \frac{3p_1 p_2}{2(2p_1 + p_2)} \end{aligned} \tag{9}$$

To find the critical value of the extraction rate β^*, we enforce current continuity at the exit of the lattice

$$\begin{aligned} \beta^* \frac{2p_1 + p_2}{3(p_1 + p_2)} &= \frac{p_1 p_2}{2(p_1 + p_2)} \\ \Rightarrow \ \beta^* &= \frac{3p_1 p_2}{2(2p_1 + p_2)} \end{aligned} \tag{10}$$

The fact that $\alpha^* = \beta^*$ is a reflection of the particle-hole symmetric intrinsic to the two-rate TASEP model.

A similar approach (see Appendix B) can used to find current and density approximations in the parameter regimes where the entry or exit rate limits the rate of particle transport through the lattice. First addressing the entry limited region we find

$$\begin{aligned} J_\alpha &= \frac{\alpha(p_1(p_2 - \alpha) - \alpha^2 + \sqrt{4p_1^2(p_2 - \alpha)\alpha + (p_1 p_2 - p_1\alpha + \alpha^2)^2})}{2p_2(\alpha + p_1)} \\ \sigma_1 &= \frac{2\alpha p_2 + \alpha^2 + p_1(\alpha + p_2) - \sqrt{4p_1^2(p_2 - \alpha)\alpha + (p_1 p_2 - p_1\alpha + \alpha^2)^2}}{2p_2(\alpha + p_1)} \\ \sigma_2 &= \frac{\alpha}{p_2} \end{aligned} \tag{11}$$

Similarly, the solution in the exit-limited phase is

$$
\begin{aligned}
J_\alpha &= \frac{\beta(p_1(p_2-\beta)-\beta^2+\sqrt{(4p_1^2(p_2-\beta)\beta+(p_1p_2-p_1\beta+\beta^2)^2)}}{2p_2(\beta+p_1)} \\
\sigma_1 &= 1-\frac{\beta}{p_2} \\
\sigma_2 &= \frac{p_1(p_2-\beta)-\beta^2+\sqrt{4p_1^2(p_2-\beta)\beta+(p_1p_2-p_1\beta+\beta^2)^2}}{2p_2(\beta+p_1)}
\end{aligned}
\tag{12}
$$

III. MONTE CARLO SIMULATIONS

Extensive Monte Carlo simulation were performed to validate the various analytical models presented in the previous section. As we expected the densities in the lattice to vary significantly as the internal hopping rates were varied, we decided to base our Monte Carlo code on the BKL continuous-time algorithm [16]. The BKL algorithm has the advantage of maintaining a constant computational efficiency over a wide range of particle densities.

The magnitude of the finite size effect in our simulations was estimated by running lattices of varying lengths. For lattices at least one thousand sites long, the MC results were found to systematically deviate from the known TASEP results ($p_1 = p_2$) by less than half a percent. As a result, we used lattices containing approximately 1000 sites for all our simulations. The simulations were run for 4×10^9 steps, which was sufficient to reproduce the known TASEP results in lattices much longer than our 1000 site standard. In all simulations, p_1 was normalized to 1. Finally, to ensure an unbiased sampling of the lattice states, a linear-congruential pseudorandom number generator with a period of 2×10^{18} was used [17].

A. Currents

The maximal current results (Figs 2, 3) show the expected qualitative behavior with a low current for small values of p_2 and a value of 1/4 when $p_2 = p_1 = 1$. In Fig 2 the boundary-limited current predictions (Eqn 11) were used to generate a prediction for the maximal current as a function of p_2. This was accomplished by maximizing J in Eqn 11 with respect to α. Consistent with our expectations, we find that the two cluster MF approaches, and the finite-segment mean field approach, provide better approximations to the Monte-Carlo results than does the simplest mean-field method. The relatively poor performance of the simple mean field model can be ascribed to the strong pair correlations present in the two-rate TASEP, which the simple MF model completely fails to capture. The 2-cluster maximal current mean field clearly performs best when $p_2/p_1 \approx 1$. In this, limit the model is essentially the normal single rate TASEP, and the expected pair correlations between adjacent p_1 and p_2 sites are negligible. As simple mean field methods are known to provide exact results for the standard TASEP, the ability of the 2-cluster MF to provide accurate results in this region is not surprising. In contrast the boundary-limited 2-cluster MF performs best when $p_2 \ll p_1$ where the correlations between adjacent p_1 and p_2 sites are expected to be strongest (although the known TASEP results are returned with $p_1 = p_2$). Nonetheless in the limit $p_2 \to 0$, the *relative* error increases for all the mean field methods.

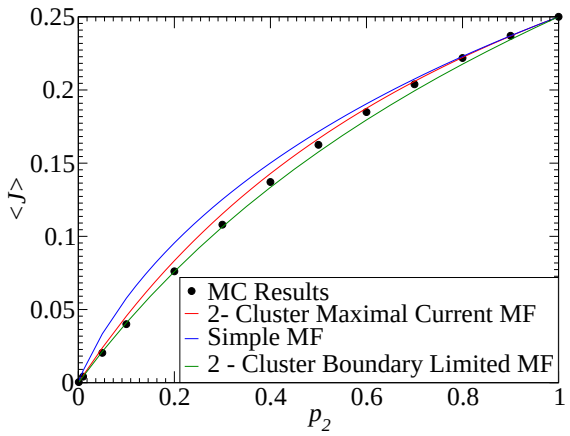

FIG. 2: Current in the maximal current phase for a $T = 2$ dual-rate TASEP. The results from the 2-cluster boundary limited MFT were produced by maximizing J in (11) with respect to α.

B. Densities

Referring to Figs 5 through 7, we find the finite-segment MF, and both 2-cluster mean field methods provide excellent matches to the simulation results. The densities produced by the maximal current 2-cluster MFT, the boundary limited 2-cluster MFT, and the finite segment method are all within 5% of the MC results, with the FSMFT results improving with increased segment length. For all three approaches the quality of the agreement is relatively uniform over all the values of p_2, though the maximal current 2-cluster mean field results do tend to have an increased relative error at smaller values of

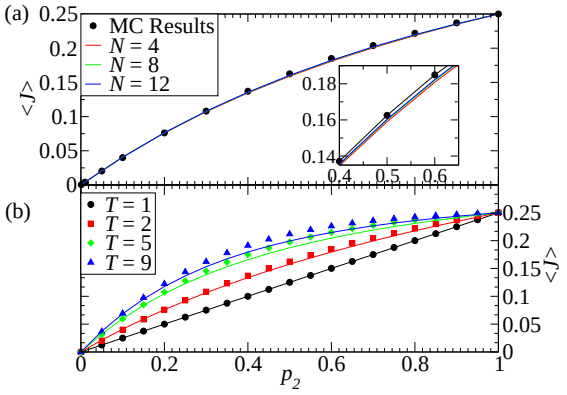

FIG. 3: (a) The effect of increasing segment length on the quality of the FSMFT estimates of the maximal current in a $T = 2$ dual-rate TASEP. The points are the Monte-Carlo simulation results, the lines are the FSMFT estimates. For segment lengths greater than or equal to twice the period, the quality of the current estimate shows only marginal improvement with increasing length. (b) Maximal currents for dual-rate TASEPs of various periods. The FSMFT estimates were produced using a single period of the lattice as the finite segment. While providing reasonable estimates, the deviation between the MC and FSMFT results increases as the period (T) increases. As seen in (a), this increase in error can be mitigated by increasing the number of periods included in the finite-segment.

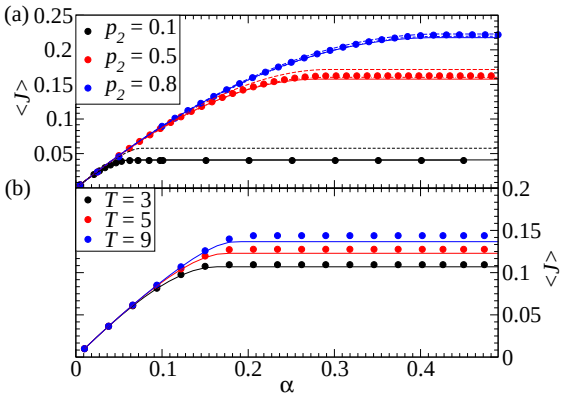

FIG. 4: (a) Current profiles along the α direction in the $T = 2$ dual-rate TASEP phase plane. The solid lines were produced using (11), the dashed lines were produced using (4), and the dotted-dashed lines were produced using an $N = 8$ FSMFT approach. (b) Current profiles for dual-rate TASEPS of various periods with $p_2 = 0.25$. The FSMFT results (solid lines) were produced using an $N = T$ FSMFT approach. From the plot we can observe the second order character of the entry-limited to maximal current transition.

p_2 where the correlations between adjacent sites are expected to be strongest. In contrast, the simple mean field approach shows very significant deviations from the experimental results particularly the small p_2 limit. Given the simple mean field method's inability to capture correlations in the density between adjacent fast and slow sites, the poor performance of this method at small values of p_2 is not unexpected.

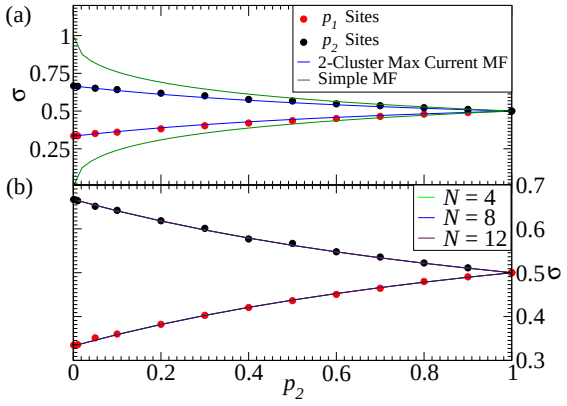

FIG. 5: (a) Densities from the simple MF method, the 2-cluster mean field method, and the Monte Carlo (MC) simulations for a $T = 2$ dual-rate TASEP. The simple mean field assumption results in the largest error for small values of p_2 where we expect the density correlation between adjacent sites to be large. (b) Results produced by the FSMFT method for various segment sizes.

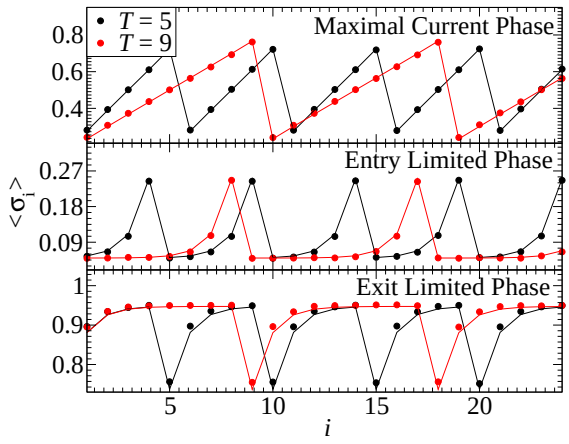

FIG. 6: The bulk density profiles for $T = 5$ and $T = 9$ dual-rate TASEPS with $p_2/p_1 = 0.2$, in all three current phases. The plots show the good agreement between the Monte-Carlo (points) and $N = T$ FSMFT (solid lines) results.

C. Correlations

Looking at the maximal-current density correlations displayed in Figs 8 and 9, we see that the pair correlation $\langle \tau_1 \tau_2 \rangle$ is very large for small values of p_2 and approaches zero as $p_2 \to p_1$. The size of this pair correlation for small p_2 confirms our intuition that the slow sites dominate the dynamics of the system, and is consistent with the maximal current assumption.

Figure 9(b) indicates that in the maximal current phase the $\langle \tau_2 \tau_1 \rangle$ pair correlation is negligible. The absence of significant correlation in Fig 9(b) and the rapid

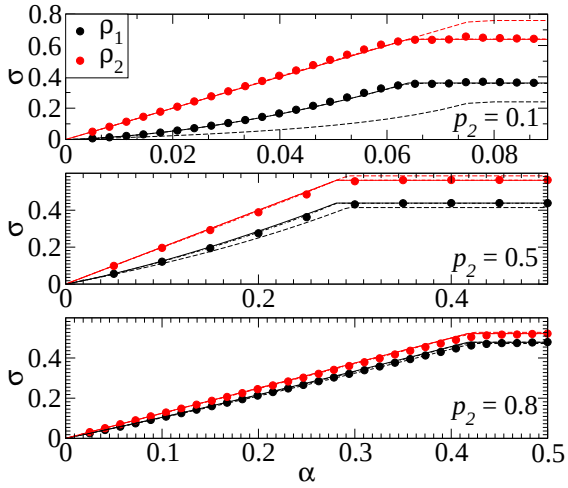

FIG. 7: The density profile along the α direction in the $T = 2$ dual-rate TASEP phase plane. The solid lines were produced using (11), the dashed lines were produced using (4), while the dotted-dashed lines were produced by an $N = 8$ finite-segment MF approach. Note that although solution for σ_2 is the same in Eqns. (4) and (11), the predicted value of α^* differs between the two mean field theories. This is the reason for the significant difference between the σ_2 profiles predicted by the two mean field methods at small values of p_2.

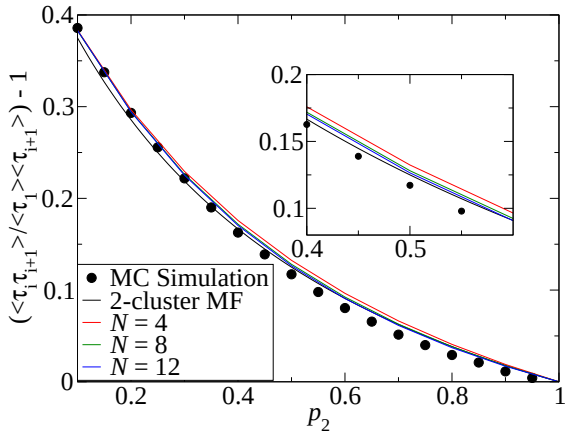

FIG. 8: The pair correlation function produced by the MC simulations and the various MF approximations for the $T = 2$ dual-rate TASEP. As expected the 2-cluster mean field approach provides a very good match to the MC results. As expected, the results produced by the segment MF improve with an increasing segment length.

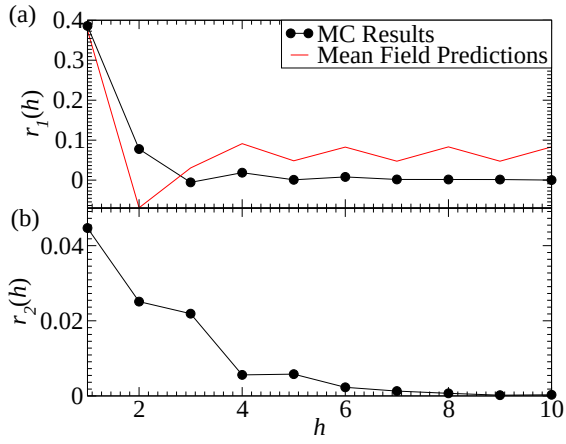

FIG. 9: The pair correlation function produced by the MC simulations for the $T = 2$ dual-rate TASEP. Plot (a) displays the correlation between fast sites and their neighbors to the right, while (b) does the same for slow sites. In both plots $p_2 = 0.1$ In (a), the pair correlation ($h = 1$) is quite strong indicating that the slow sites are acting to limit the rate of transport through the lattice consistent with the maximal current assumption. Conversely, (b) shows that slow sites are essentially uncorrelated with their neighbors to the right.

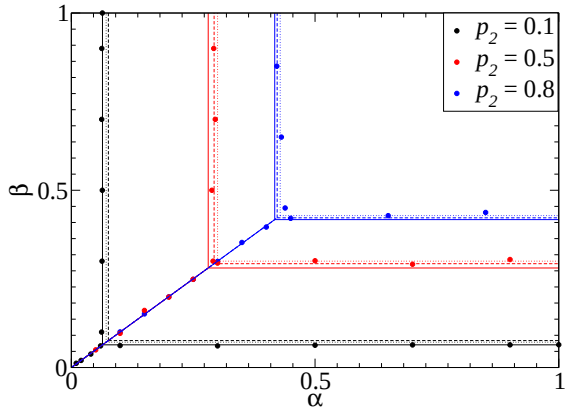

FIG. 10: The phase diagram for the $T = 2$ two-rate TASEP. The dashed lines are produced by the simple mean field theory (Eqns 4, 6). The dotted lines are produced by the maximal current 2-cluster method (Eqn 8), and the solid lines are produced by the boundary-limited mean field method (Eqns 11, 12).

decay of the correlation function in Fig 9(a) indicates that the dynamics of the two-rate TASEP are essentially the dynamics of a set of successive, and nearly independent (p_1, p_2) unit cells. While the correlation functions in Fig. 9 show longer range behavior, sites separated by more than two intervening lattice sites are essentially uncorrelated. Despite the maximal current 2-cluster method's ability to provide highly accurate estimates for the pair correlation function (Fig. 8), the 2-cluster method generates predictions for the current and density that carry small but significant error particularly for small p_2. To seek the source of this error, we must consider the correlation profile produced by the maximal-current 2-cluster method. If we consider two lattice sites separated by h intervening lattice sites, the general pair correlation function can then be formed as follows:

$$r(h) \quad = \quad \langle \tau_i \tau_{i+h} \rangle / \langle \tau_i \rangle \langle \tau_{i+1} \rangle - 1$$

Where :

$$\langle \tau_i \tau_{i+h} \rangle \; = \; \frac{\sum_{\tau_i} P(1,\tau_1) \left[\Pi_{i=2}^{h-2} P(\tau_i, \tau_{i+1}) \right] P(\tau_{h-1}, 1)}{\sum_{\{\tau_i\}} \Pi_{i=1}^{h-1} P(\tau_i, \tau_{i+1})} \tag{13}$$

Referring to Fig. 9, we see that while the 2-cluster method provides good estimates for the pair correlation function, its predictions for the correlation profile are relatively poor. While the correlation profile produced from the results of the MC simulations decays rapidly to zero, the results are not negligible for $h = 2, 3$, and thus we expect these small longer range correlations to have some effect on the current and density of the two site TASEP. The failure of the maximal current 2-cluster method to capture these weak longer range correlations may be responsible for the increasing error in the mean field current and densities with decreasing p_2.

D. Phase Diagram

The phase diagram derived from simulations is displayed in Fig 10, along with the phase boundaries predicted by the various mean field methods. The Monte Carlo phase boundaries were computed by taking numerical derivatives of the current as a function of α and β and locating any clear discontinuities in the derivatives. The dual-rate TASEP retains the general form of the standard TASEP phase-diagram, and the order of the transitions remains unchanged; first order between the high and low density regimes, and second order between the boundary limited and maximal current regions. The most significant deviation from the standard phase diagram is the increase in the maximal current region which accompanies a decrease in one of the hopping rates (p_2 in our example). Physically, the maximal current region is defined as the region of the (α, β) parameter space where the internal motions determine the net particle flow through the lattice. The increase in the area of the maximal current phase with decreasing p_2 is then expected as we naturally require α or β to be less than p_2 in order to enter a boundary limited region.

Despite the varying degrees of success in predicting accurate steady state currents and densities, all three mean field approaches predict the phase boundaries within approximately 12% error. As was observed in the mean field predictions for the steady state currents and densities, the boundary-limited 2-cluster mean field approach provides the best predictions at small values of p_2/p_1, while the maximal current mean field method excels when $p_2 \approx p_1$. We also note that the phase transitions predicted by the boundary-limited 2-cluster approach were determined numerically by maximizing J in Eqns (11) and (12)

IV. CONCLUSION

We have developed and presented four separate approximate methods to compute the the current and densities of totally asymmetric exclusions processes involving two internal hopping rates. Moreover, we have extensively simulated the two-rate TASEP and have thoroughly explored its phase diagram. We find that the dual-rate TASEP retains the three phases found in the standard TASEP model. Within each of these phases the best of our mean field theories provide highly accurate, albeit not exact, predictions for the particle currents and densities. In particular, a maximal current phase 2-cluster mean field theory was developed that provides accurate estimates (Eqn. 8) for the current and the density (Figs. 2,5) and the pair correlation function $\langle \tau_1 \tau_1 \rangle$ (Fig. 8). Similarly, in the boundary limited phases a simplified 2-cluster MF method was introduced (Eqn. 11, 12), which produced accurate estimates for the boundary currents, and reasonably accurate estimates for the maximal currents (Fig. 4). In addition to the generally inferior simple mean field approach (Eqns. 2, 4, 6), we have developed a primarily numerical mean field method that we have termed the finite segment mean field method. This method can rapidly produce accurate estimates for the currents and densities in all three phases of the dual-rate TASEP. Additionally, the finite-segment method shows promise as a means of producing accurate estimates for the current and the density of TASEPs with hopping rates that vary spatially in a manner more complex than the periodic pattern described in this paper.

Given the success of mean field theories in predicting the current and density in the standard TASEP, as well as various extended TASEPs, the inability of our mean field approaches to provide exact results is noteworthy. Comparison of our best mean field predictions of the density correlation function with the Monte Carlo results (Figs 8, 9) indicate that while the 2-cluster mean field approach accurately captures the strong correlation between adjacent fast and slow lattice sites, the method does not account for the weaker, but still significant, longer range correlations. An extension to a three or four site cluster model may yield better analytic results.

Acknowledgments

GL acknowledges support from the Natural Science and Engineering Research Council of Canada. TC acknowledges support from the NSF (DMS-0206733), and the NIH (R01 AI41935). ABK acknowledges support from the Camille and Henry Dreyfus New Faculty Awards Program (under Grant No. NF-00-056), from the Welch Foundation (under Grant No. C-1559), and from the US National Science Foundation through the grant CHE-0237105. The authors thank B. Bergersen, and G. Patey for valuable comments on the manuscript and C. Greif for his assistance with the Arnoldi diagonalization

routines.

APPENDIX A: THE FINITE-SEGMENT MEAN FIELD METHOD

Here we give a detailed description of the the algorithm underlying the finite segment mean field method, and focus on using the method to solve for the currents and densities in the maximal current phase. Consider a finite lattice containing N sites and a whole number of $(p_1, p_1, \ldots, p_2)$ periods. Working under the assumption that the bulk densities in the lattice are periodic and inherit the same periodicity as the movement rates, we focus on a single period. We then define the effective rate of injection into this finite segment of the lattice and the effective rate of extraction in terms of the unknown particle densities inside the segment. This yields $\alpha_{\text{eff}} = p_2\sigma_{k+1}$ and $\beta_{\text{eff}} = p_2(1-\sigma_1)$. Using these rates and the known values of p_1 and p_2 we can build the transition matrix for the master equation describing the motion of the particles in our T-site finite-segment. Letting N be the number of sites in the finite segment, and $\vec{R}_i$ be the movement rate for site i in the segment, the algorithm to construct the master equation transition matrix is (Fig. 11):

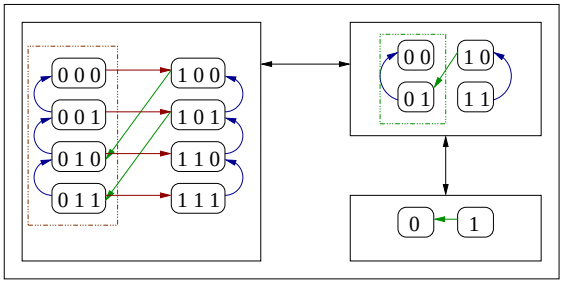

FIG. 11: The steps in the algorithm to generate the transition matrix for a TASEP model. For the purposes of illustration a three site model has been used. To begin we treat each possible occupancy of the lattice as a bit pattern, and label the state with the corresponding decimal value. For example given that `011` is the binary representation of `3`, we label the state with particles occupying the second and third lattice sites as *state 3*. Next we divide the states into two groups; states where the first lattice site is occupied *(1-states)*, and states where the first lattice site is empty *(0-states)*. Regardless of the number of lattice sites in the TASEP, the transitions between the two classes of states *always* occur between the first half of the *1-states* and the second half of the *0-states* (the straight green arrows in the figure). To determine the remaining transitions we call the algorithm recursively on both the *1-states* and the *0-states*, making sure to ignore the highest order bit (*i.e.* the leftmost lattice site). Finally we add in the trivial transitions between each *0-state* and each *1-state* that are the result of injection at the left edge of the lattice (the red arrows in the diagram). With the connectivity of the states fully enumerated, assigning the appropriate rate p_i to each of the transitions is straightforward.

1. Label every state of the N-site finite segment with a number determined by the occupancy of the lattice sites. For example, an $N = 3$ lattice with only the last site filled (*ie* an occupancy of 001), is said to be in *state 1*, while the same lattice with the last two sites filled (an occupancy of 011) is said to be in *state 3*.

2. Separate the states generated in step 1 into two groups; the states where the left-most lattice site is empty (the *0-states*), and the state where the left-most lattice site is full (the *1-states*).

3. Enumerate the transitions between the 1-states and the 0-states. The transitions will always be the movements that take the system from the lowest 2^{N-2} 1-states to the highest 2^{N-2} 0-states. The rate of these transitions is $\vec{R}_l$, where l is the current depth of the recursion (see step 4).

4. Recurse on the 0-states and then on the 1-states, ignoring the leftmost site (*ie* with each recursion of the algorithm, we reduce the length of the segment by 1), or stop if the current segment length is $N = 1$.

5. Once the recursion specified in steps 1 through 4 has completed, enumerate all the trivial transitions between the 0-states and the 1-states that occur at rate α (*ie* the state transitions due to particle injection on the left).

With the master equation constructed by this algorithm, we can then compute the densities in the finite segment, apply a self consistency condition on the densities, and subsequently compute the current in terms of the hopping rates p_1 and p_2. Thus utilizing the state enumeration scheme and algorithm described in Fig. 11, we generate and solve the following equations

$$\begin{aligned} \mathbf{M}(\{\sigma_\mathbf{i}\}, \mathbf{p_1}, \mathbf{p_2})\vec{V} &= 0 \\ \textstyle\sum_{i=2^{N-1}+1}^{2^N} V_i(\{\sigma_i\}, p_1, p_2) &= \sigma_1 \\ \textstyle\sum_{i=1}^{2^{N-1}} V_{2i-1}(\{\sigma_i\}, p_1, p_2) &= \sigma_N \end{aligned} \tag{A1}$$

In Eqn (A1), $\mathbf{M}$ is the transition matrix, while V_i is the probability of finding the finite-segment in occupancy state $0 < i < (2^N - 1)$ (see Fig. 11). When applying the finite-segment mean field approach, (A1) is solved iteratively until a fixed point in the densities is reached. Using the results from (A1) we can compute the current from the expression $J = \alpha_{\text{eff}} \sum_{i=1}^{2^{N-1}} V_i$ (or $\beta_{\text{eff}} \sum_{i=1}^{2^{N-1}} V_{2i-1}$). Additionally, the finite-segment method can be extended to treat the boundary limited dual-rate TASEP by fixing $\alpha_{\text{eff}} = \alpha$ or $\beta_{\text{eff}} = \beta$ as appropriate, and applying the density self-consistency condition at the end of the finite-segment that lies in the interior of the TASEP lattice. While a simple and effective approach, the exponential increase in the size of the transition matrix with the

length of the segment quickly renders (A1) analytically untreatable. As a result we chose to solve (A1) numerically using a simple fixed-point iteration scheme. Employing the fast Arnoldi-method eigensolvers in the well-known ARPACK linear-algebra software library [18], we could easily treat segments containing ~ 20 lattice sites.

APPENDIX B: CLUSTER MEAN FIELD METHODS

We begin the derivation of the current and density approximations displayed in Eqn (8) by considering the two site probability $P(\tau_i, \tau_{i+1})$. Here, τ_i refers to the occupancy of site i, and is equal to 1 if the site is occupied, 0 if the site is empty. The time evolution of the occupancy state of any two adjacent sites in a TASEP will depend on the two sites themselves along with the site immediately to the left and the right of the two site grouping (Fig 12b).

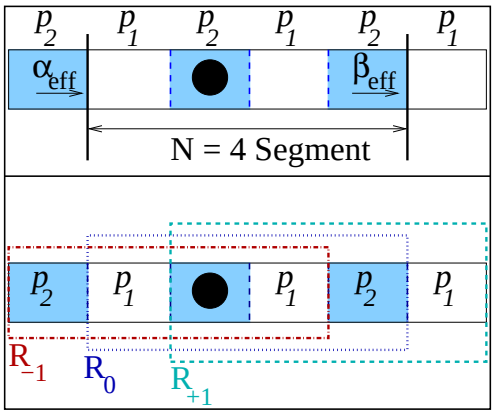

FIG. 12: The lattice site groupings used in the two enhanced mean field approaches. (a) The arrangement used for an $N = 4$ finite segment mean field (MFT) approach. The master equation for the state of the four marked lattice sites is solved exactly. The four sites are coupled to the rest of the lattice by assuming an effective injection rate of $\alpha_{\rm eff} = p_2\sigma_2$ on the left, and an effective extraction rate of $\beta_{\rm eff} = p_2(1-\sigma_1)$ on the right. (b) The arrangement of lattice sites used in the 2-cluster mean field theory. The two lattice sites of interest are the central two sites in grouping R_0. Groupings R_{+1} and R_{-1} are produced by shifting the boundaries of the group R_0 one lattice site to the right, and one lattice site to the left respectively. To generate a second set of equations, we simply interchange all the p_1 and p_2 sites, while keeping the groupings R_{+1}, R_0, and R_{-1} the same.

Thus the master equation for the two site probability is [15]

$$\begin{aligned}
&\frac{dP(\tau_i,\tau_{i+1})}{dt} = \\
&\sum_{\tau_{i-1},\tau_{i+2}} Q(\tau_{i-1},\tau_{i+1},\tau_i,\tau_{i+2})(p_1\delta_{\tau_i,0}\delta_{\tau_{i+1},1}) \\
&-Q(\tau_{i-1},\tau_i,\tau_{i+1},\tau_{i+2})(p_1\delta_{\tau_i,1}\delta_{\tau_{i+1},0}) \\
&+\sum_{\tau_{i-1},\tau_{i-2}} P(\tau_{i-2},\tau_i,\tau_{i-1},\tau_{i+1})(p_2\delta_{\tau_i,1}\delta_{\tau_{i-1},0}) \\
&-P(\tau_{i-2},\tau_{i-1},\tau_i,\tau_{i+1})(p_2\delta_{\tau_{i-1},1}\delta_{\tau_i,0}) \\
&+\sum_{\tau_{i+2},\tau_{i+3}} P(\tau_i,\tau_{i+2},\tau_{i+1},\tau_{i+3})(p_2\delta_{tau_{i+1},0}\delta_{\tau_{i+2},1}) \\
&-P(\tau_i,\tau_{i+1},\tau_{i+2},\tau_{i+3})(p_1\delta_{\tau_{i+1},1}\delta_{\tau_{i+2},0})
\end{aligned} \tag{B1}$$

As we have incorporated two different hopping rates into the TASEP model we are forced to deal with two sets of probabilities; the first ($P(\tau_i,\tau_{i+1},\tau_{i+2},\tau_{i+3})$) refers to the probability of having configuration $(\tau_i,\tau_{i+1},\ldots)$ given that the first site (site i) is a p_1 site. The second probability term ($Q(\tau_i,\tau_{i+1},\tau_{i+2},\tau_{i+3})$), is the probability of configuration $(\tau_i,\tau_{i+1},\ldots)$ when the first site is a p_2 site. Now we assume we can factor the 4-site probabilities as follows

$$\begin{aligned}
P(\tau_i,\tau_{i+1},\tau_{i+2},\tau_{i+3}) &= P(\tau_i,\tau_{i+1})Q(\tau_{i+1},\tau_{i+2})P(\tau_{i+2},\tau_{i+3}) \\
Q(\tau_i,\tau_{i+2},\tau_{i+2},\tau_{i+3}) &= Q(\tau_i,\tau_{i+1})P(\tau_{i+1},\tau_{i+2})Q(\tau_{i+2},\tau_{i+3})
\end{aligned} \tag{B2}$$

And by definition we have

$$\begin{aligned}
\sigma_1 &= P(1,0)+P(1,1) \\
\sigma_2 &= Q(1,0)+Q(1,1) \\
P(0,0) &= 1-P(0,1)-P(1,0)-P(1,1)
\end{aligned} \tag{B3}$$

Thus, in the steady state we can write

$$\begin{aligned}
\frac{dP(0,0)}{dt} &= p_2\left(P(0,1,0,1)-P(1,1,0,0)\right) \\
&= p_2(P(0,1)Q(1,0)P(0,1) \\
&\quad -P(1,1)Q(1,0)P(0,0)) = 0
\end{aligned} \tag{B4}$$

Upon using (B3), we find

$$P(1,0) = \frac{\sigma_1(1-\sigma_2)-(\sigma_2-\sigma_1)^2}{1+(\sigma_2-\sigma_1)} \tag{B5}$$

The equation for $Q(1,0)$ can be found from (B5), by interchanging p_1 and p_2, as well as σ_1 and σ_2. Applying the current continuity condition $p_1P(1,0) = p_2Q(1,0)$, we then arrive at the relation

$$p_1\frac{\sigma_1(1-\sigma_2)-(\sigma_2-\sigma_1)^2}{1+(\sigma_2-\sigma_1)} = p_2\frac{\sigma_2(1-\sigma_1)-(\sigma_1-\sigma_2)^2}{1+(\sigma_1-\sigma_2)} \tag{B6}$$

We now make the substitution $\sigma_2 - \sigma_1 = k$ and define p_1 to be the larger of the two rates. Thus $\sigma_1 < \sigma_2$ and $k > 0$. Solving (B6) for σ_1, we find $\sigma_1 =$

$$\frac{\left[p_2(1-k^2) - p_1(k-1)^2\right] + \sqrt{(1-k^2)(k(p_1+p_2)-(p_1-p_2))(3k(p_1+p_2)-(p_1-p_2))}}{2k(p_1+p_2)-(p_1-p_2)} \tag{B7}$$

From (B7) we find that σ_1 is real only when $k < \frac{p_1-p_2}{3(p_1+p_2)}$ or $k > \frac{p_1-p_2}{p_1+p_2}$. Substituting (B7) into (B6) we find $J = \frac{kp_1p_2}{(p_1-p_2)-k(p_1+p_2)}$, which shows $J < 0$ for $k > \frac{p_1-p_2}{p_1+p_2}$, $J > 0$ for $0 < k < \frac{p_1-p_2}{p_1+p_2}$, and $\frac{dJ}{dk} = \frac{p_1p_2(p_1-p_2)}{(k(p_2+p_1)+(p_2-p_1))^2} > 0 \forall k$ Since J must be positive, σ_1 must be real, and J is monotonically increasing, the maximum value of the current must occur when $k = \frac{p_1-p_2}{3(p_1+p_2)}$. Substituting this value of k into (B7), we arrive at (8).

An analogous approach can be used to find current and density estimates in the entry and exit limited regions. Considering the entry limited case first, we find the following master equation for the occupancy of the first two sites in the lattice:

$$\begin{aligned}
\frac{dP(0,0)}{dt} &= -\alpha P(0,0) + p_2 P(0,1)(P(0,0)+P(0,1)) \\
\frac{dP(0,1)}{dt} &= -\alpha P(0,1) - p_2 P(0,1)(P(0,0)+P(0,1)) \\
&\quad + p_1 P(1,0) \\
\frac{dP(1,0)}{dt} &= \alpha P(0,0) + p_2 P(1,1)(P(0,0)+P(0,1)) \\
&\quad - p_1 P(1,0) \\
\frac{dP(1,1)}{dt} &= -p_2 P(1,1)(P(0,0)+P(0,1)) + \alpha P(0,1)
\end{aligned} \tag{B8}$$

In writing (B8) we have assumed that the occupancy probabilities $P(\tau_1, \tau_2)$ do not vary significantly as a function of position near the entrance of the lattice. This assumption is analogous to that used with the standard TASEP in the boundary limited region where the density is assumed to be essentially constant. Applying the normalization condition on the probabilities $P(\tau_i, \tau_{i+1})$ and solving (B8) generates the results displayed in (11). An analogous approach yields the current and densities in the exit limited regime (Eqn. 12).

[1] B. Derrida, E. Domany, and D. J. Mukamel, Phys. A **26** 1493 (1992)
[2] B. Derrida, M. R. Evans, V. Hakim,and V. Pasquier, J. Stat. Phys. **69** 667 (1993)
[3] B. Derrida, Physics Reports **301** 65 (1998)
[4] G. M. Schutz, E. Domany, J. Stat. Phys. **72** 277 (1993)
[5] C. T. MacDonald, J. H. Gibbs, and A. C. Pipkin, Biopolymers **6** 1 (1968)
[6] G. Lakatos, T. Chou, J. Phys. A. **36** 2027 (2003)
[7] L. B. Shaw, R. K. P. Zia, and K. H. Lee, Phys. Rev. E **68**, 021910 (2003)
[8] T. Chou, D. Lohse, Phys. Rev. Lett. **82** 3552 (1999)
[9] M. Schreckenberg, A. Schadschneider, K. Nagel, N. Ito, Phys. Rev. E. **51** 2939 (1995)
[10] T. Nagatani, J. Phys. A. **26**, 6625 (1993)
[11] S. M. Block, Cell **93** 5 (1998)
[12] M. Schliwa, G. Woehlke, Nature **422** 759 (2003)
[13] W. Hua, J. Chung, J. Gelles, Science **295** 844 (2002)
[14] A. Parmeggiani, T. Franosch, E. Frey, Phys. Rev. Lett. **90** 086601-1 (2003)
[15] D. Chowdhury, J. S. Wang, Phys. Rev. E. **65** 046126 (2002)
[16] A. B. Bortz, M. H. Kalos, and J. L. Lebowitz, J. Comp. Phys. **17** 10-18 (1975)
[17] W. H. Press, S. A. Teukolsky, W. T. Vetterling, B. P. Flannery *Numerical Recipes in C, Second Edition* (Cam-

bridge: Cambridge University Press, 1995)
[18] R. B. Lehoucq, D. C. Sorensen, and C. Yang, ARPACK Users' Guide: Solution of Large-Scale Eigenvalue Problems with Implicitly Restarted Arnoldi Methods, (SIAM, Philadelphia, 1998)
[19] J. Krug, Phys. Rev. Lett. **67** 1882 (1991)
[20] B. Derrida and M. R. Evans, in *Nonequilibrium Statistical Mechanics in One Dimension*, (Cambridge University Press, Cambridge, 1997)
[21] A. B. Kolomeisky, G. M. Schutz, E. B. Kolomeisky, and J. P. Straley, J. Phys. A **31** 6911 (1998)
[22] G. A. Gutman, G. W. Hatfield, Proc. Nat. Academy Sci. **86** 3699 (1989)
[23] G. Tripathy and M. Barma, Phys. Rev. E. **58** 1911 (1998)
[24] A. B. Kolomeisky, J. Phys. A **31** 1153-1164 (1998)
[25] If the instantaneous lattice occupancy is $\tau_i \in [0, 1]$, the average density at site i in the steady state is defined as $\sigma_i =< \tau_i >$